Article No. jmbi.1999.2777 available online at http://www.idealibrary.com on IDEAL® J. Mol. Biol. (1999) 289, 799–813

JMB

Global Structure and Flexibility of Hairpin Ribozymes with Extended Terminal Helices

Dietmar Porschke[1]*, John M. Burke[2] and Nils G. Walter[2]

[1]*Max Planck Institut für Biophysikalische Chemie D-37077, Göttingen, Germany*

[2]*Department of Microbiology and Molecular Genetics University of Vermont Burlington, VT 05405, USA*

**Corresponding author*

Global structure and flexibility of three different hairpin ribozyme constructs have been analyzed by measuring their electric dichroism decay in various buffers at temperatures between 2 and 30 °C. The hairpin ribozyme is characterized by two independently folding domains A and B that are connected through a hinge and have to interact to enable catalysis. The analyzed constructs feature extended terminal helices 1 and 4 with 27 and 25 bp, respectively, to increase the sensitivity of the molecular rotational diffusion time constants with respect to the interdomain bending angle. Constructs HP1 and HP2 cannot cleave because of a $G_{+1}A$ change at the 3′-side of the cleavage site; in HP1 the helices 2 and 3 that flank the hinge form a continuous double helical segment; in HP2 and HP3, a six nucleotide bulge confers flexibility to the expected bending site; HP3 is a cleavable form of HP2 with a G_{+1}-base. For comparison, a standard RNA double helix with 72 bp was included in our analysis. The dichroism decay curves of the hairpin constructs after pulses of low electric field strengths can be fitted to single exponentials τ_s, whereas the curves after pulses of high field strengths require two exponentials. In all cases, time constants increase with RNA concentration, indicating intermolecular interactions. Extrapolation of the τ_s values measured in standard buffer (50 mM Tris (pH 7.5) and 12 mM $MgCl_2$) to zero RNA concentration provide values of 112, 93, and 73 ns for HP1, HP2 and HP3, respectively, at 30 °C, indicating increasingly compact structures. The 72 bp RNA reference under corresponding conditions did not show a dependence of its decay time constant on the RNA concentration nor on the field strength; its time constant is 175 ns (standard buffer, 30 °C). The observation of two relaxation processes for the hairpin constructs at high field strengths indicates stretching to a more elongated state; the fast process with a time constant of the order of 50 ns is assigned to reversion of stretching, the slow process to overall rotation. The overall rotational time of the stretched state at 20 °C is close to that for a completely stretched rigid state; at 30 °C the experimental values are around 70 % of that expected for a completely stretched rigid state, indicating flexibility and/or residual bending. Bead models were constructed to simulate dichroism decay curves. The time constants observed for the 72 bp RNA are as expected for a rigid rod with a rise of 2.8 Å per base-pair. Based on this rise per base-pair for models of a V and a Y-shape, we estimate average bending angles of 80(±20)° and 105 (±25)°, respectively, for the catalytically active hairpin ribozyme HP3. The energy required for stretching is of the order of the thermal energy.

Keywords: RNA dynamics; RNA folding; rotational diffusion; transient electric dichroism; bead model simulation

Abbreviations used: dsRNA, double-stranded RNA; EtBr, ethidium bromide; RBP, rise per base-pair; SAP, segment addition polarization; TEB, transient electric birefringence; TED, transient electric dichroism; (−)sTRSV, negative strand of tobacco ringspot virus satellite.

E-mail address of the corresponding author: dpoersc@gwdg.de

0022-2836/99/240799–15 $30.00/0

Introduction

In the late 1980s, several naturally occurring, self-cleaving catalytic RNA motifs were discovered, including the hammerhead, hairpin, hepatitis delta and VS ribozymes. They all can be truncated and engineered to cleave a substrate site-specifically *in trans*, generating 2′,3′-cyclic phosphate and 5′-OH termini (for the most recent review, see Sigurdsson *et al*., 1998). Based on this observation, applications as therapeutic agents to disable undesired intracellular RNAs (such as cancer gene mRNAs or retroviral genomes) were envisioned (Haseloff & Gerlach, 1988; Sarver *et al*., 1990; Ojwang *et al*., 1992). In parallel with the development of ribozymes as an advanced antisense gene therapy, intensive research was initiated to understand the relationship between structure and function in these catalytic RNAs, with the ultimate goal to control and optimize their intracellular activity.

Our current knowledge on the structures of these rather small catalytic RNA motifs is at very different stages. While there are several crystal structures available for the hammerhead ribozyme (Pley *et al*., 1994; Scott *et al*., 1995), including two of early and late intermediates of the reaction pathway (Scott *et al*., 1996; Murray *et al*., 1998), and a recently reported crystal structure of the hepatitis delta virus ribozyme (Ferre-D'Amare *et al*., 1998), our understanding of the hairpin ribozyme structure at the molecular level is still limited (Walter & Burke, 1998). Through extensive studies of natural and artificial phylogenies, mutational analysis and chemical probing (reviewed by Burke *et al*., 1996), the secondary structure of this endonucleolytic motif from the negative strand of tobacco ringspot virus satellite ((−)sTRSV) RNA and related plant viroids has been determined (Figure 1(a)). The minimal ribozyme-substrate complex is composed of two independently folding domains A and B, connected by a flexible hinge. The substrate binds to the substrate-binding strand of the ribozyme to form domain A (Figure 1(a)). Both domains are characterized by an internal loop between two helices. The loops carry virtually all catalytically relevant nucleotides (Figure 1(b)). UV crosslinking experiments on domain B (Butcher & Burke, 1994) and two NMR structure determinations of the isolated domains A (Cai & Tinoco, 1996) and B (Butcher *et al*., 1999) in the absence of Mg^{2+} indicate extensive non-canonical base-pairing across the loops (reviewed by Walter and Burke, 1998). From previous linker insertion studies (Feldstein & Bruening, 1993; Komatsu *et al*., 1994), a catalytically crucial Mg^{2+}-dependent interaction between the loops has been suggested, accompanied by a sharp bend around the hinge (Figure 1(b)). Recently, the folding kinetics from an extended into this docked conformation has been followed through increased fluorescence resonance energy transfer (FRET) between a donor-acceptor pair coupled to the ends of the approaching domains (Walter *et al*., 1998). Using time-resolved FRET, the equilibrium distribution between the extended and docked conformers was analyzed as a function of interdomain junction design (Walter *et al*., 1999).

The bending angle at the two-way junction of the interacting domains is crucial to understanding the global architecture of the active hairpin ribozyme-substrate complex. Molecular modelling studies based on distance constraints from interdomain crosslinking have suggested a bending angle of 80° between the helical axes of stems A and B (Earnshaw *et al*., 1997; Pinard *et al*., 1999). Here, we were interested in directly acquiring information on this angle using transient electric dichroism (TED). TED in its quantitative form has been used previously for the analysis of tRNAs (Porschke & Antosiewicz, 1990) and for studies of DNA (Porschke, 1991) and DNA-protein complexes (Porschke *et al*., 1988; Antosiewicz & Porschke, 1988; Meyer-Almes *et al*., 1994). Its sensitivity and quantifiability should make TED a well suited tool for studying hairpin ribozyme structure. In addition, developments in its experimental setup (Porschke, 1991) allow measurements with constructs of moderate lengths at salt concentrations, as they are typically used in ribozyme studies (e.g. 50 mM NaCl, 50 mM Tris-HCl, 12 mM $MgCl_2$).

A closely related method, called transient electric birefringence (TEB), has been used widely by Hagerman and co-workers to analyze global RNA structure (Hagerman & Amiri, 1996), including studies on artificial RNA two-way junctions (Zacharias & Hagerman, 1995a), three-way junctions from 5 S rRNA (Shen & Hagerman, 1994), 16 S rRNA (Orr *et al*., 1998) and the hammerhead ribozyme (Amiri & Hagerman, 1994, 1996; Gast *et al*., 1994) as well as four-way junctions in tRNA (Friederich *et al*., 1995, 1998; Leehey *et al*., 1995) and the *trans*-activation response (TAR) element of human immunodeficiency virus (Zacharias & Hagerman, 1995b).

For both TED and TEB experiments on RNA in solution, the RNA molecules are (partially) oriented by applying a short electric field pulse. As a result of the net orientation, the RNA solution becomes optically anisotropic: the absorbance depends on the polarization plane of light. After removal of the field, the transient orientation and anisotropy is gradually lost due to rotational diffusion of the molecules. In the case of TED, the anisotropy decrease is monitored as a decay in linear dichroism, in the case of TEB as a decay in birefringence (Fredericq & Houssier, 1973). Information on global RNA structure can be obtained from the time constants of this decay, which reflect the rotational diffusion of the RNA and are strongly dependent on its size and shape.

To increase the sensitivity of the molecular rotational diffusion time constants with respect to the bending angle between domains A and B of the hairpin ribozyme-substrate complex, we extended its terminal helices H1 and H4 to 27 and 25 bp, respectively (Figure 1(c)). Complexes were generated from transcribed RNA, with either a

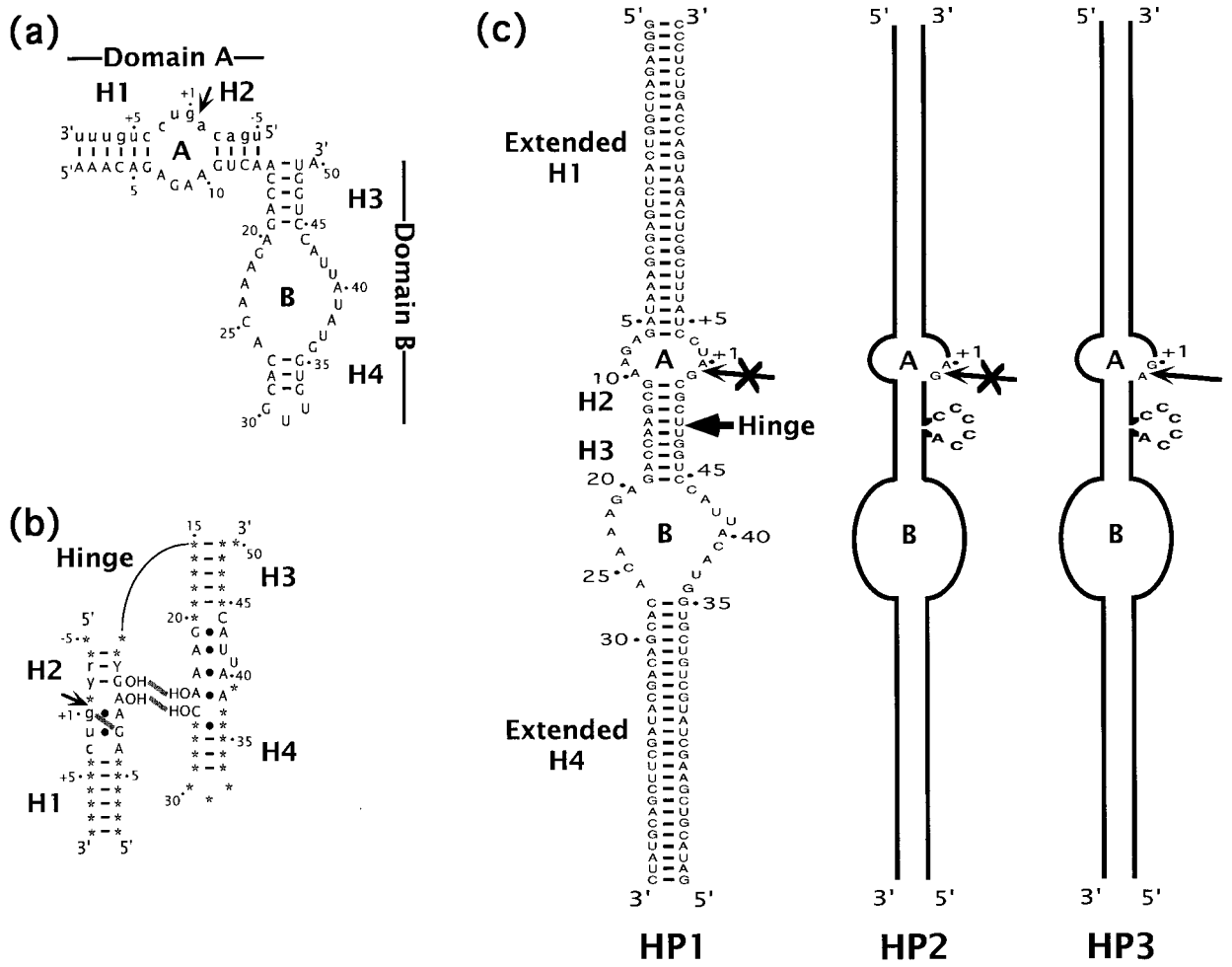

Figure 1. Hairpin ribozyme structure. (a) Primary and secondary structure of the naturally occurring wild-type hairpin ribozyme from the negative strand RNA of tobacco ringspot virus satellite. The two independently folding domains A and B each consist of two helices (H1, H2 and H3, H4; black lines, Watson-Crick base-pairing), flanking internal loops A and B, respectively. Ribozyme nucleotides are numbered 1 to 50. The external substrate (lower case letters, nucleotides numbered −5 to +9) is bound in the A domain. Its cleavage site is marked by an arrow. (b) Consensus sequence and bent structure. *In vitro* selection and mutational analysis have defined essential nucleotides, mostly in the loop regions; r, purine; y or Y, pyrimidine. Stars indicate variable bases. A sharp bend around the hinge between domains A and B enables the conserved regions to approach each other. (c) The three constructs employed in this study for TED measurements. H1 and H4 are extended, the substrate strand (with cleavage site) is linked to the ribozyme either directly (HP1) or through a six nucleotide bulge (HP2 and HP3), and sequence changes around the cleavage site either produce a catalytically active (arrow) or inactive (crossed out arrow) structure

direct linkage or a six nucleotide bulge between substrate and ribozyme, creating different potentials for flexibility in the hinge. In addition, the complexes either contained a guanosine or an adenosine base immediately 3′ to the cleavage site (position +1), with G_{+1} being a requirement for domain docking (Walter *et al.*, 1998; Hampel *et al.*, 1998). A closely related RNA double helix with 72 bp was used as a reference for the quantitative assignment of relaxation processes. Using these various constructs, we were able to identify relaxation processes in the hairpin constructs due to stretching and bending motions around the hinge (at high field strengths) as well as orientational randomization caused by rotational diffusion (at both high and low field strengths). The time constant for the bending motion reveals dynamics of the bulged regions, while the overall rotational diffusion time constant can be translated into an apparent average interdomain bending angle on the basis of bead model simulations. A catalytically active construct shows the most compact structure with an interdomain angle of 80(±20)°, representing a first direct experimental assessment of the global architecture of the hairpin ribozyme.

Results

Design, electrophoretic and catalytic characterization of ribozyme-substrate complexes

Three different transcribed hairpin ribozyme constructs were used, termed HP1 to HP3, in

which the 5′ end of the substrate is linked to the ribozyme 3′ end to generate stable, terminally extended ribozyme-substrate complexes (Figure 1(c)). This arrangement has been shown to result in catalytically active complexes, provided that the link contains at least a three nucleotide bulge (Feldstein & Bruening, 1993). In HP1, the link does not contain any bulged nucleotides, resulting in a rigid fusion of H2 and H3 into a continuous helical element. In addition, the bases of positions −1 and +1 (flanking the scissile bond) are exchanged, placing an adenosine residue in position +1 instead of a guanosine residue. This mutation has been shown to render a substrate non-cleavable, due to interference with domain docking (Walter *et al*., 1998; Hampel *et al*., 1998). The corresponding ribozyme-substrate complex adopts a single, extended conformation (Walter *et al*., 1999). In HP2, a six nucleotide linker is introduced between substrate and ribozyme, creating a potentially flexible hinge between domains A and B of the complex (Figure 1(c)). However, this construct still contains the $G_{+1}A$ mutation deleterious for tertiary structure formation. In HP3, finally, both the six nucleotide bulge in the hinge as well as the G in position +1 are present, giving this complex full potential for docking of its domains A and B and cleavage. A similar construct, but with short terminal helices and a deoxy modification in position −1 to block reaction chemistry, was shown to yield 74 % docked and 26 % of a more extended complex (Walter *et al*., 1999).

We ensured homogeneity of our annealed two-strand constructs by analysis on non-denaturing polyacrylamide gels. Similar analyses frequently have been used to obtain qualitative information on the global structure of double-stranded RNAs with bulges (e.g. Bassi *et al*., 1995; Zacharias & Hagerman, 1995a; Friederich *et al*., 1998). In Figure 2(a), the electrophoretic mobility patterns of the three constructs HP1 to HP3 are shown in the presence of the metal-ion chelator EDTA and of magnesium ions, respectively. In all cases a single, EtBr-stained band is observed, indicating that the global structures indeed fold homogeneously, a prerequisite for a successful structure determination. Patterns under both conditions are analogous, with HP3 migrating between the more mobile HP1 and the less mobile HP2. Hagerman and co-workers have observed that bulges in double-helical RNAs reduce electrophoretic mobility by inducing bends in the RNA structure (Zacharias & Hagerman, 1995a). Our observations, therefore, suggest that the introduction of a bulge into the hinge between domains A and B results in some bending of HP2 and HP3 *versus* the unbulged HP1, both in the absence and presence of Mg^{2+}.

To ensure that our constructs, in principle, are catalytically active, we performed cleavage assays on the 3′ strand of HP3 carrying the essential G_{+1}. Mutagenesis of this guanosine residue results in complete loss of catalytic activity (Chowrira *et al*., 1991; results not shown). Subnanomolar concentrations of the 3′ strand of HP3 were cleaved both in the context of the complete HP3 construct and by a hairpin ribozyme *in trans*, with identical rates of 0.035 min^{-1} at 25 °C under standard single turnover conditions (50 mM Tris-HCl (pH 7.5), 12 mM MgCl2, buffer T-Mg; Figure 2(b)). The final extent of cleavage differs considerably (28 % *versus* 61 %), suggesting a different equilibrium between cleavage and re-ligation. It is likely that this difference is due to the considerably longer binding arms of the cleavage products in HP3, that completely prevent dissociation of both the 5′ and 3′ product from the complex (data not shown). A similar construct to HP3 with a G_{+1} at the cleavage site, but lacking the six nucleotide bulge, termed HP0, was catalytically inactive under these conditions (Figure 2(b)), demonstrating that cleavage in the HP3 construct requires a flexible hinge to dock domains A and B, and does not occur intermolecularly (*in trans*). However, at the micromolar concentrations used in TED experiments, this ribozyme-substrate complex can be cleaved *in trans* (data not shown). Because of this cleavage we focussed our efforts on a comparison of the HP1 to HP3 constructs and give only a brief summary of results obtained for HP0.

Analysis of TED curves

Application of electric field pulses to micromolar solutions of the three hairpin constructs led to an increase of the transmission of light polarized parallel with the field vector, indicating a negative dichroism. Measurements at the magic angle orientation of polarized light did not indicate field-induced changes of light intensity within the limits of experimental accuracy. Thus, all dichroism signals can be attributed to molecular orientation, without contributions from absorbance changes by field-induced conformational changes (Porschke, 1996).

The dichroism decay curves obtained for the three hairpin constructs were least-squares fitted with single exponentials, or with double exponentials if necessary (Figure 3). Residuals for fits with single exponentials were small for decay curves recorded after pulses of low field strength (40 kV/cm); they were pronounced, however, for decay curves recorded after pulses of high field strength (90 kV/cm). This is evident, e.g. in the sum of residuals, which decreases only slightly (20 to 40 %) upon increasing the number of exponentials from one to two for decay curves measured after 40 kV/cm pulses, whereas the corresponding decrease is in the range of fivefold for decay curves measured after 90 kV/cm pulses (Figure 3). This observation indicates a single process associated with dichroism decays at low field strength, and two processes at high field strength.

Measurements of the hairpin constructs at different RNA concentrations *c* showed a slight, but sig-

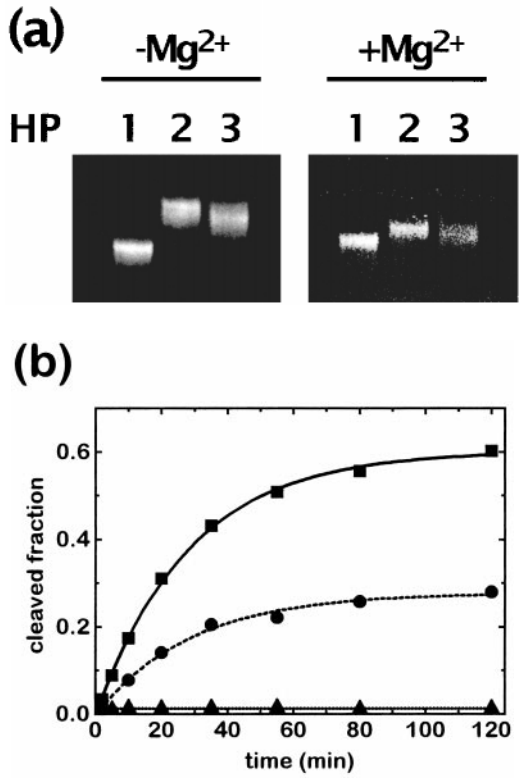

Figure 2. Electrophoretic and catalytic properties of the three hairpin ribozyme constructs. (a) Migration pattern on a non-denaturing gel in the absence or presence of magnesium ions as described in Materials and Methods. (b) Catalytic properties of construct HP3. The 3′ strand of HP3 was cleaved either by a hairpin ribozyme (construct SV5 EH4 Rz; Esteban *et al.*, 1997) *in trans* (squares) or by the 5′ strand of HP3 *in cis* (circles). The data were least-squares fitted to the single exponential equation $y = y_0 + A(1 - e^{-t/\tau})$ with $1/\tau = 0.035\ \text{min}^{-1}$ in both cases, but amplitudes of $A = 0.61$ and 0.28, respectively (continuous and broken lines). When a modified form of the 3′ strand lacking the six nucleotide bulge was incubated with the 5′ strand of HP3, no cleavage was observed (triangles and dotted line).

nificant increase of the exponential time constants τ_s with increasing c (Figure 4). This concentration dependence is likely due to interactions between the RNA molecules that are expected to slow their rotational diffusion. We obtained the rotational diffusion time constants in the absence of these interactions by linear extrapolation to zero RNA concentration. Because of the relatively small concentration dependence, the correction resulting from extrapolation is also relatively small (cf. Figure 4) and, thus, potential errors due to the correction are not critical. Time constants obtained by this procedure for HP1 to HP3 in various buffers and at different temperatures are shown in Table 1 for low field strength, and in Table 2 for high field strength. Accuracies of time constants were estimated, mainly from multiple independent experiments, to 10 % for single-exponential fits and to 30 % and 20 % for the fast and slow processes of double-exponential fits, respectively.

The reference double-strand (dsRNA) with 72 bp (containing the same 5′ strand with a fully complementary 3′ strand) also showed a negative dichroism, but its dichroism decay curves could be fitted by single exponentials throughout all electric field strengths. As a result and because the dichroism decay was slower than that of the hairpin constructs, the decay time constants of the 72 bp RNA could be determined at an estimated accuracy of ±4 %. These time constants did not show any dependence on the nucleotide concentration up to 3 μM under different conditions (Table 3).

Experiments on the construct HP0 demonstrated that it is quite similar to construct HP1. HP0 showed a field strength dependence of its dichroism decay curves, with single exponential decays at low field strength and double exponential decays at high field strength. The single exponential time constants τ_s increase with increasing RNA concentration. Extrapolation of the data obtained in buffer T-Mg at 20 °C to zero RNA concentration provided a time constant $\tau_s = 182$ ns. Dichroism decay time constants of HP0 somewhat larger than that of HP1 were also observed in other buffers/temperatures. It is remarkable that the $G_{+1}A$ mutation induces a detectable and reproducible change of the dichroism decay time, even though this change remains relatively small.

TED measurements at low field strengths reveal differences in rotational diffusion properties

The dichroism decay time constants in Table 1 have several noteworthy qualitative features. First, the time constants for constructs HP1, HP2, and HP3 (152 ns, 122 ns and 116 ns, respectively, at 20 °C in cleavage buffer T-Mg) are much smaller than that for the reference dsRNA (233 ns). Furthermore, they are significantly different from one another, suggesting that their associated structures are distinct. Under all conditions tested, HP3 exhibits the smallest constant, consistent with displaying the most compact structure. This is quite striking, since all three constructs utilize the same 5′ half and differ only in a few nucleotides of their 3′ halves. HP1 has a rigid continuous helix 2/3 segment (Figure 1(c)) so that it is forced into an extended structure, consistent with its rotational diffusion being slow (large time constant). Since HP2 and HP3 share the same six nucleotide bulge in the interdomain hinge (Figure 1(c)), the additional slight decrease in rotational diffusion time constant from HP2 to HP3 has to be attributed to its changed cleavage site sequence. The difference between HP2 and HP3 becomes more pronounced with increasing temperature (93 ns *versus* 73 ns at 30 °C, respectively).

Second, HP3 displays quite different rotational diffusion properties dependent on the ionic con-

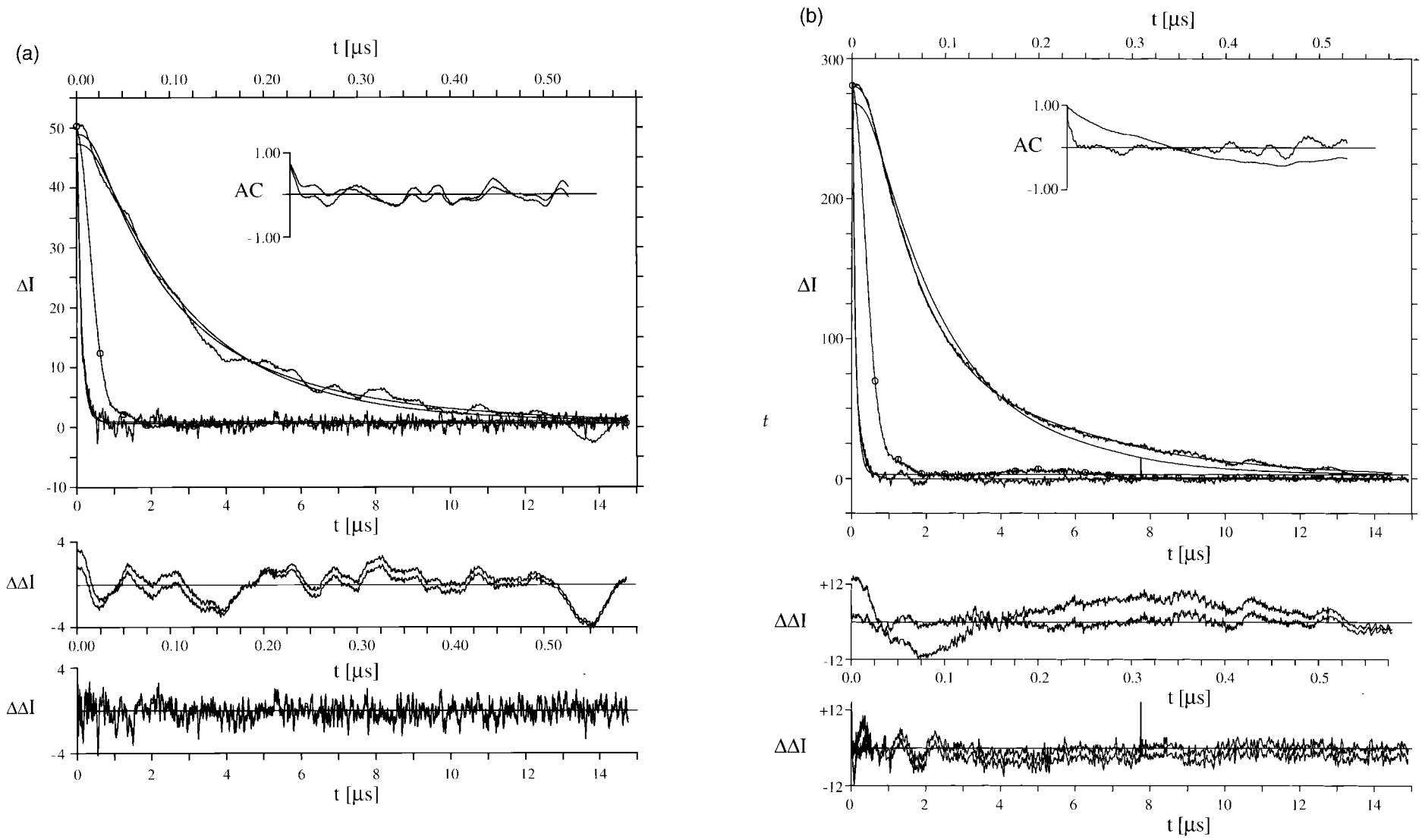

Figure 3. Dichroism decay curves (ΔI as a function of time t) measured for HP3 at 20 °C in buffer T-Na after an electric field pulse of (a) 40 kV/cm and of (b) 80 kV/cm, shown at two different time-scales. The lines without noise represent least-squares fits with one and two exponentials; the line marked with circles, which is shown only for the short time-scale, represents the birefringence signal used for deconvolution. The lower panels show the residuals $\Delta\Delta I$ for the one and the two-exponential fits in the two time-scales. The insert in the upper panel shows the autocorrelation AC of the residuals for the one and the two-exponential fits; note the distinct systematic deviation of AC from the zero level for the one-exponential fit in (b).

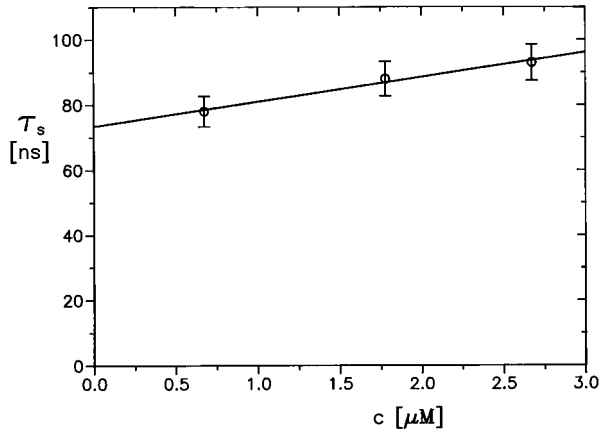

Figure 4. Dichroism decay time constants τ_s of HP3 measured at 30 °C in buffer T-Mg at different concentrations *c*. The straight line represents a linear regression with the intercept at 73 ns.

ditions and temperature in solution (Table 1). In buffer T-Na at pH 7.5 and 20 °C, in the presence of 50 mM NaCl for proper secondary structure formation, rotational diffusion is faster (time constant 94 ns) than in buffer T-Mg with 12 mM $MgCl_2$ as salt component (time constant 116 ns). This effect is not simply caused by differences in ionic strength, since buffer T-Mg-Na with both 50 mM NaCl and 12 mM $MgCl_2$ yields an intermediate rotational diffusion time constant (106 ns). It is well known that magnesium, but not low concentrations of sodium ions, lead to folding of a catalytically competent hairpin ribozyme-substrate complex such as HP3 from an open into a docked conformation (Walter *et al.*, 1998, 1999; Hampel *et al.*, 1998). However, the docked form can be expected to be rather more compact; therefore, intuitively a decreased rotational diffusion time constant would be expected.

Table 1. Dichroism decay time constants τ_s of the three different ribozyme constructs HP1, HP2 and HP3 as obtained from single-exponential fits, corresponding to the limit of low electric field strength

Construct	*t* (°C)	Buffer	τ_s (ns)
HP3	2	T-Na	168
HP3	2	T-Mg-Na	243
dsRNA	2	T-Mg-Na	437
HP1	20	T-Mg	152
HP2	20	T-Mg	122
HP3	20	T-Mg	116
HP3	20	T-Na	94
HP3	20	T-Mg-Na	106
dsRNA	20	T-Mg	233
HP1	30	T-Mg	112
HP2	30	T-Mg	93
HP3	30	T-Mg	73
dsRNA	30	T-Mg	175

These values are compared with time constants obtained for double stranded RNA with 72 base-pairs (dsRNA). Estimated accuracy: ±10 % for HP1, HP2 and HP3; ±4 % for dsRNA (cf. the text).

Table 2. Dichroism decay time constants τ_1 and τ_2 (estimated accuracy $\tau_1 \pm 30\,\%$; $\tau_2 \pm 20\,\%$) for the three different ribozyme constructs in buffer T-Mg measured in the limit of high electric field strength

Construct	*t* (°C)	τ_1 (ns)	τ_2 (ns)
HP1	20	70	238
HP2	20	62	260
HP3	20	37	208
Straight rod	20	-	230
HP1	30	26	115
HP2	30	41	149
HP3	30	37	114
Straight rod	30	-	177

For comparison, the decay time constant expected for a straight rod with dimensions corresponding to a double helix of the *A*-type with 72 bp was calculated (rise per base-pair 2.8 Å, helix radius 12.5 Å; procedure as described by Tirado *et al.*, 1984). τ_1 is attributed to hairpin bending and τ_2 corresponds to overall rotational diffusion of (partially) stretched configurations (see the text).

Another parameter influencing the observed rotational diffusion time constants is the flexibility of the molecule. As demonstrated in our initial catalytic characterization in T-Mg buffer (Figure 2(b)), HP3 will cleave to 28 % completion without dissociation of the reaction products due to their long binding arms. Under our conditions, after annealing the strands in Mg^{2+}-containing buffer and preincubation in the TED cell, this equilibrium is reached. The ternary complex of ribozyme with bound cleavage products stays in the active docked conformation (Walter *et al.*, 1998, 1999), but an increased flexibility due to the introduced nick could affect the rotational diffusion time constant.

We therefore attempted to obtain information on a hairpin ribozyme-substrate complex before cleavage. At 2 °C, cleavage is considerably slower than at 20 °C; with an activation energy of 22 kcal/mol (Hampel & Tritz, 1989; A. R. Banerjee, J. A. Esteban & J.M.B., unpublished results) and a reaction rate constant of 0.035 min^{-1} at 25 °C (see above), reaction rate constants at 2 °C and 20 °C can be estimated to 0.0016 min^{-1} and 0.019 min^{-1}, respectively. Therefore, the rotational diffusion time constant at 2 °C in buffer T-Mg-Na (with the ribozyme substrate complex assembled in Mg^{2+}-free buffer, and Mg^{2+}, that is essential for catalytic activity, only subsequently added at 2 °C) should

Table 3. Dichroism decay time constants (estimated accuracy ±4 %) for the reference RNA helix with 72 bp in the buffers T-Na, T-Mg and T-Mg-Na

t (°C)	T-Na	T-Mg	T-Mg-Na
2		433(244)	437 (246)
20	244	233	221
30	183 (238)	175(227)	

To demonstrate the temperature dependence of the measured values independent of the usual decrease of water viscosity with increasing temperature, the time constants were normalized to 20 °C (values in parentheses) using the standard temperature/viscosity conversion factor for water viscosity.

Table 4. Electro-optical data simulated for hairpin constructs according to V and Y-models with different bending angles

Angle (deg.)	V-Model					Y-Model
		Induced		Permanent		
	τ_{max}	τ_a	$(\Delta\varepsilon/\varepsilon)_\infty$	τ_a	$(\Delta\varepsilon/\varepsilon)_\infty$	τ_{max}
40	56.0	54.1	−0.803	54.7	−0.801	63.8
60	65.2	50.2	−0.609	52.5	−0.607	67.1
80	86.4	48.2	−0.370	42.7	−0.369	73.7
100	109.8	77.3	−0.370	*109.5	−0.116	84.8
120	132.2	123.6	−0.608	*132.1	+0.122	95.2
150	159.8	159.4	−0.876	169.1	+0.389	
180	168	168	−0.974			

τ_{max} is the maximal of the five exponential time constants; induced and permanent denote the different dipole models (cf. the text); τ_a is the average time constant obtained by fitting of the calculated dichroism decay by a single exponential function; the values marked by * represent the second of two time constants obtained from biphasic dichroism decay curves (cf. the text); $(\Delta\varepsilon/\varepsilon)_\infty$ is the limit value of the dichroism calculated according to the model. The time constants are calculated for 30 °C using a viscosity of 0.7975×10^{-3} kg m^{-1} s^{-1}.

reflect mainly uncleaved complex. Still, the dichroism decay time constant is higher in the presence of Mg^{2+} than in its absence (243 ns *versus* 168 ns), indicating that the observed difference might relate to the difference in how monovalent and divalent cations interact with the negatively charged RNA backbone.

It should be noted that the bending angle between domains A and B of the hairpin ribozyme-substrate complex can be estimated more quantitatively based on simulations using bead models (see below). However, any angle will be ''apparent'' in nature, because both fixed bending and flexibility contribute to the observed average hydrodynamic dimensions. Some information on the contribution of flexibility can be derived from the dependence on the electric field strength (see below).

TED measurements at high field strengths yield information on stretching and bending motions around the hinge as well as on rotational diffusion properties of the stretched state

At high field strength, experimental dichroism decays of the hairpin constructs HP1, HP2, and HP3 were best fitted with two exponentials. A set of these time constants obtained in buffer T-Mg is reported in Table 2. Similar results were obtained in buffers T-Na and T-Mg-Na. In analogy to corresponding results for DNA double helices (Diekmann *et al*., 1982; Porschke, 1989), the fast process can be assigned to elastic bending after field induced stretching: dipolar forces induced by external electric fields stretch bent configurations; after pulse termination the stretched configurations relax back to their equilibrium state. The slow process can be assigned to overall rotation of partially stretched configurations; depending on the time constants of bending, stretched configurations may still contribute to the overall rotational diffusion process. In the case of DNA double helices, bending amplitudes strongly increased with chain length, but were negligible for chain lengths below 90 bp. Thus, our finding that bending amplitudes were not observed for the RNA double helix with 72 bp is consistent with previous results for fully double-stranded DNA.

Our data at high field strength indicate, therefore, that the bends of HP1 to HP3 can be stretched with only a low energetic penalty in the order of the thermal energy (cf. discussion below). In the case of construct HP3, stretching might interfere with domain-docking interactions, which then were similarly weak. The resulting, more extended states of all three constructs appear to be stretched out completely at 20 °C, as inferred from a comparison with the theoretical relaxation time of a straight rod of corresponding dimensions (Table 2). At 30 °C, the time constants τ_2 are around 70 % of that expected for a completely stretched rigid state, indicating flexibility and/or residual bending. The difference of the τ_2 values at 20 and 30 °C may be explained by different relaxation time constants of bending: according to this interpretation stretching is reverted at a higher rate at 30 °C than at 20 °C.

The electric dichroism value for full orientation also provides information on the shape of a molecule. Because the electric field pulses were limited to 200 ns duration, electric dichroism was far from saturation even at the highest field strength (90 kV/cm). The reduced dichroism values observed at the end of the 90 kV/cm pulses were in the range of −0.04 to −0.08, depending on the type of buffer. The highest dichroism values were observed in buffer T-Na, whereas the lowest values were found in buffer T-Na-Mg. The dichroism increase with increasing field strength was also far from saturation. Finally, the acceleration of the dichroism increase during the pulses by increasing electric field strengths was very limited. Taken together, these observations indicate that the dipolar energy induced by the electric field pulses remained rather close to the thermal energy. These conditions do not allow one to determine the exact electric dichroism at complete orientation. We estimate limiting values of the electric dichroism for HP3 from the amplitudes of exponential fits to rise curves to −0.25, −0.35 and −0.5 for the buffers T-Mg at 30 °C, T-Na-Mg at 20 °C and T-Na at 20 °C, respectively (estimated accuracy ±50 %). Because of their limited accuracy, these values may only be used as an approximate indication for the structure of the hairpin ribozyme construct, but allow a qualitative comparison with results from bead model simulations (see below). The dichroism amplitudes observed for the 72 bp RNA were higher than those for the hairpin constructs, in spite of the relatively slow rotational diffusion. Due to the slow rotational diffusion, the dichroism rise curves at the end of the field pulses were too

far from their stationary levels, such that these stationary levels could not be extrapolated.

Bead model simulations yield quantitative information on hairpin ribozyme structure

The dichroism decay time constants indicate that all three hairpin ribozyme constructs under standard conditions do not exist in fully extended (straight rod) configurations as the double-stranded control RNA, but instead form more compact structures. To translate TED data into quantitative information on global structure, simulations by bead models were used. For these models we exploited the existing knowledge on hairpin ribozyme global structure (Walter & Burke, 1998), indicating that both loops A and B form rather well-defined structures with extensive non-canonical base-pairing (Cai & Tinoco, 1996; Butcher *et al*., 1999). In our simulations, we assumed that both loops A and B have similar dimensions as *A*-type RNA helices. Cleavage requires that loops A and B approach each other for specific interactions, accompanied by bending between them. The bend occurs at the bulge between helices 2 and 3, at the center of constructs HP2 and HP3 (Figure 1(c)). Thus, a first set of models was constructed using two straight segments: one of these segments includes helix 1, loop A and helix 2 with an effective length of 35 bp, whereas the other includes helix 3, loop B and helix 4 with an effective length of 37 bp. The length of these segments is approximated under the assumption of an *A*-type helical structure with a 2.8 Å rise per base-pair (Arnott *et al*., 1973; Saenger, 1984; Dock-Bregeon, 1989; Holbrook *et al*., 1991; Cruse *et al*., 1994; Wahl *et al*., 1996). These two segments are connected at the site corresponding to the bulge with various bending angles. An example of such a V-model with a bending angle of 80° is shown in Figure 5(a).

In addition to the V-models, theoretical electro-optical data were calculated for a series of Y-models. These models have been designed according to the hairpin structure proposed by Earnshaw *et al*. (1997), where loops A and B are in close contact with each other. This ''core'' of the structure remains constant in the various Y-models, whereas helices 1 and 4 are attached to the core at different angles (cf. Figure 5(b)). Note that this structure, thus, implies bends in loops A and B.

According to theory, dichroism decay curves of rigid bodies contain up to five exponential functions (Wegener *et al*., 1979). The time constants of these exponentials are defined by the dimensions and the geometry of the body. The amplitudes associated with the exponentials are dependent on the electrical and optical parameters. Usually it is not possible to separate the five exponentials, because their superposition is described in most cases within experimental accuracy by a single average exponential (Antosiewicz *et al*., 1992; Antosiewicz & Porschke, 1995). The average exponential

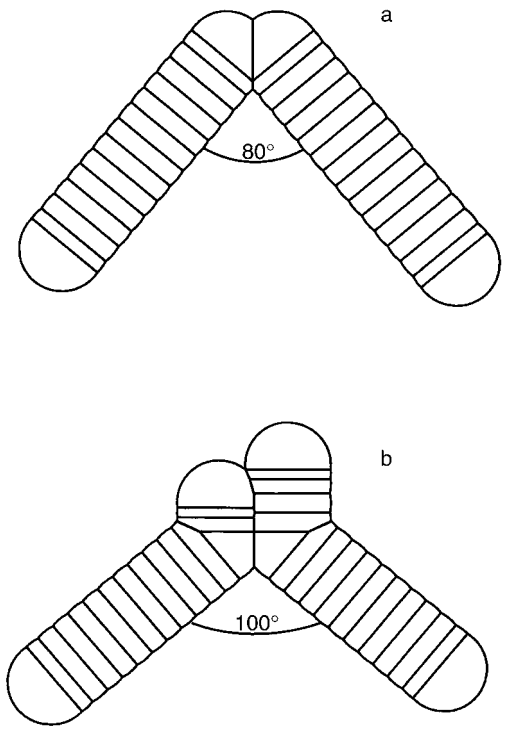

Figure 5. (a) Example of a bead model of the V-type with a bending angle of 80°. The diameter of the beads is 25 Å. (b) Example of a bead model of the Y-type with a bending angle of 100°. The diameter of the beads is 25 Å.

time constant τ_a obtained from simulated decay curves corresponds to the time constant τ_s derived from the experimental data by single-exponential fitting. As shown in Table 4, the τ_a values are affected by the choice of the electric parameters (Antosiewicz *et al*., 1992; Antosiewicz & Porschke, 1995); the electric parameters determine the orientation of the molecules in the external electric field and, thus, the amplitudes associated with the five individual exponentials.

The electric parameters of RNA molecules of complex structures cannot be calculated quantitatively, but can be approximated on the basis of comparisons with other biological macromolecules including DNA (Porschke, 1997). The models used for the present simulations are non-symmetric with respect to two of three axes (cf. Figure 5), corresponding to a non-symmetric distribution of the phosphate charges and resulting in a permanent dipole moment. The magnitude of this dipole moment depends on the residual charges on the phosphate groups, which are expected to be relatively small in the presence of magnesium ions. We used a residual charge per phosphate unit corresponding to 3% of the elementary charge (cf. Materials and Methods). Under these conditions, the permanent dipole moments for the various models are relatively small and may be dominated by the induced dipole. The components of the polarizability tensor were estimated on the

basis of experimental data obtained for DNA double helices. The polarizability in the direction perpendicular to the symmetry plane, corresponding to the plane of Figure 5(a) and (b), is assumed to be negligible. The polarizability in the other two directions has been assigned by tensorial addition of the contributions of helical segments, which were calculated on the basis of experimental data obtained for DNA double helices (equation (1); Porschke, 1997).

Theoretical dichroism decay curves were simulated for models of the Y and the V-shapes with different bending angles using both permanent and induced dipole parameters (cf. Table 4 and Figure 6). In most cases these curves could be fitted by single exponentials at a satisfactory accuracy. Because experimental data are subject to noise, the individual contributions in the corresponding experimental decay curves cannot be separated. In some cases of calculated decay curves, however, the amplitudes of contributions to the decay curves are in opposite direction and, thus, separation would also be possible, if observed experimentally. These cases are indicated in Table 4 and in Figure 6, where the time constants for the slow processes are given. The simulated dichroism decay time constants τ_a are affected by the electric parameters. Tensorial addition of segment contributions represents just one of different models that may be used for the estimation of the polarizability tensor. It is likely that this model underestimates the polarizability in the direction of maximal extension of the molecules. Approximate calculations using higher polarizabilities in the direction of maximal extension show that under these conditions the average time constants τ_a approaches the maximal time constant τ_{max}. Therefore, we used the time constants τ_{max} as the upper limit and τ_a, from the segment addition polarization (SAP) model, as the lower limit for the assignment of bending angles.

A comparison of the experimental time constants with the time constants simulated for the V and Y-models can be used to derive a range of average bending angles consistent with the experimental TED decays. The decay time constant of 73 ns measured for HP3 at 30 °C in T-Mg buffer (Table 1) suggests a bending angle of ~67°, based on the maximal time constant τ_{max} calculated for the V model for the same temperature. An upper limit of ~97° for the bending angle in the V-model is obtained from the data based on the SAP model (Figure 6(a)). Using these upper and lower limits and considering our levels of accuracy, the average bending angle for the construct HP3 in the V-model is 80 (±20)° at 30 °C in 12 mM Mg^{2+}. The corresponding average bending angle in the Y-model is 105 (±25)° (Figure 6(b)). Because the Y-models imply that part of the RNA segments are in close contact, it is reasonable that the bending angles obtained according to the Y-models are larger than those derived from the V-models.

The results derived from the dichroism decay time constants were confirmed by a comparison of

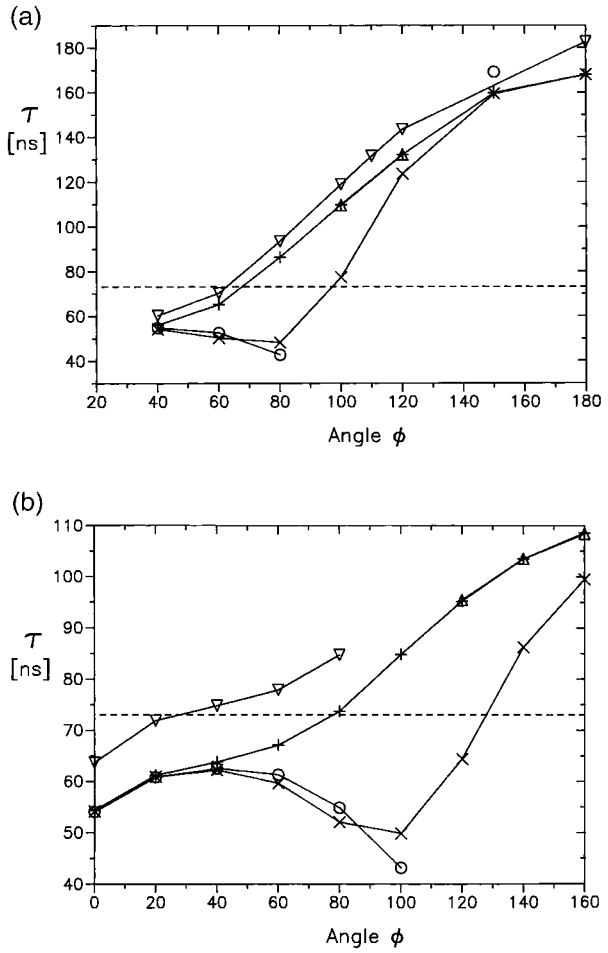

Figure 6. Time constants calculated from bead model simulations according to the (a) V-model and the (b) Y-model at 30 °C for different bending angles ϕ. Results obtained with RBP = 2.8 Å: τ_{max}, +; τ_a obtained with segment addition polarization, ×; τ_a obtained with permanent dipole moments, o; τ_2 representing the slower of two relaxation processes with opposite amplitudes obtained with permanent dipole moments, △; results obtained with RBP = 2.9 Å: τ_{max}, ▽. The broken line represents the experimental dichroism decay time constant for construct HP3 at 30 °C in buffer T-Mg.

observed and calculated limit values of the dichroism $(\Delta\varepsilon/\varepsilon)_\infty$ (Table 4 and Figure 7). Although the experimental $(\Delta\varepsilon/\varepsilon)_\infty$ values could only be approximated (see above), it is evident that the experimental $(\Delta\varepsilon/\varepsilon)_\infty$ is negative and relatively small. A comparison with simulated data based on various models demonstrates that the observed $(\Delta\varepsilon/\varepsilon)_\infty$ values in the range of −0.2 to −0.4 are consistent with bending angles in the range of 80 to 120 ° (Figure 7). Much higher absolute values of negative dichroism are expected for small bending angles between 0 and 60 °. For high bending angles approaching 180 °, the permanent dipole models predict positive $(\Delta\varepsilon/\varepsilon)_\infty$ values. However, the permanent dipole moments in this range are relatively small, and their influence is clearly exceeded by that of the induced dipole moments. This is

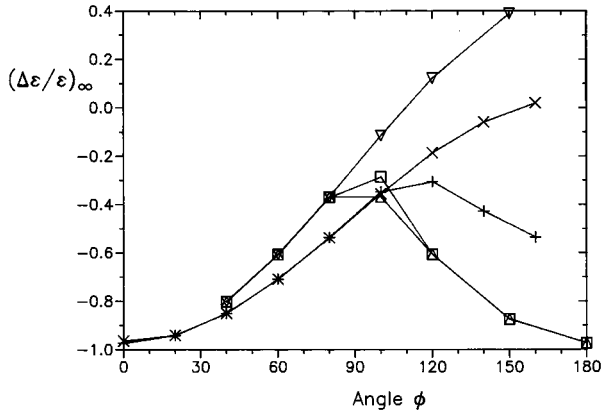

Figure 7. Limit value of the electric dichroism $(\Delta\varepsilon/\varepsilon)_\infty$ for different bending angles ϕ: V-model with segment addition polarization, △; V-model with permanent dipole moment, ▽; V-model with both permanent dipole moment and segment addition polarization, □; Y-model with segment addition polarization, +; Y-model with permanent dipole moment, ×.

demonstrated by simulations with both permanent and induced dipole moments, which reveal large negative $(\Delta\varepsilon/\varepsilon)_\infty$ values for bending angles close to 180° (cf. Figure 7). Thus, the approximate experimental $(\Delta\varepsilon/\varepsilon)_\infty$ values support average bending angles in the range around 100° for HP3 at 30 °C, in reasonable agreement with the values from rotational diffusion measurements.

Our TED data indicate that HP3 is more compact than HP1 and HP2. Using the V-models, the differences in the experimental time constants lead to increases of the average bending angles of ∼20° and ∼30° for HP2 and HP1, respectively, relative to HP3.

A special case is encountered for the Y-models, where a local maximum of τ values is found at low bending angles, both for the induced and the permanent dipole models. In this case, the experimental time constant for HP3 is consistent with an average bending angle of ∼40° for the Y-model. However, the $(\Delta\varepsilon/\varepsilon)_\infty$ value expected for this bending angle is in the range of −0.8 and, thus, not consistent with our experimental data.

The dimensions of the models are strongly influenced by the rise per base-pair (RBP) used for their construction. All the simulated data discussed above are based on an average RBP of 2.8 Å. This value is supported by our experimental data obtained for the RNA double helix with 72 bp. Because the exact value of the persistence length of RNA double helices under the conditions of our experiments is not known, it cannot be excluded that RBP is slightly higher, e.g. 2.9 Å, and that a small contribution due to flexibility leads to some reduction of the experimental time constants for the 72 bp RNA. As should be expected, an increase of RBP leads to higher values of the simulated dichroism decay time constants. Accordingly, the time constants obtained for RBP = 2.9 Å in the case of the V-models lead to average bending angles which are approximately 10° smaller than those derived from models constructed with RBP = 2.8 Å (Figure 6).

Finally, we note that the dichroism decay time constant obtained for the straight rod by the bead model simulation (Table 4, angle 180°, 168 ns at 30 °C) is slightly different from the value according to the rigid rod model (177 ns) reported by Tirado *et al*. (1984). This difference of ∼5% results from different boundary conditions and may be used as an indication for the limits of accuracy of the simulation procedure.

Discussion

We have employed transient electric dichroism (TED) to analyze global structure and flexibility of three different constructs based on the hairpin ribozyme, at different conditions of counterions and temperature. In the absence of a high-resolution structure, TED proves a valuable tool for obtaining this information for the following reasons. First, it has been possible to directly characterize the hairpin ribozyme constructs at ion concentrations, where catalysis has been studied previously. Under these conditions of physiological or slightly higher ion concentrations, where the ribozyme substrate complex is known to adopt its native conformation, TED proves to be sufficiently sensitive. Second, the instrument used for the present measurements has a particularly high time resolution, which has been used for the characterization of hairpin ribozyme bending motions. Third, a special advantage of TED over the related TEB technique is the fact that dichroism amplitudes can be calculated on the basis of structure models more easily than birefringence amplitudes. Thus, TED results can be directly used for quantitative bead model simulations to obtain structural information.

Our data present the first quantitative estimation of the global structure of the hairpin ribozyme. Although structural information is available on the separate domains A and B (Walter & Burke, 1998), their docking so far only has been characterized kinetically and thermodynamically (Walter *et al*., 1998, 1999), or by molecular modelling based on crosslinking interference studies (Earnshaw *et al*., 1997; Pinard, *et al*., 1999), and a solvent protected core of the docked complex has been mapped by hydroxyl radical footprinting (Hampel *et al*., 1998).

From the present TED experiments, several conclusions can be drawn. First, TED experiments at low field strength show that all three hairpin ribozyme constructs deviate from a straight rod structure. The molecule with the junction between domains A and B fused to a continuous helical element, HP1, exhibits the most extended structure, with an average bending angle of 110 (±10)° according to a V-shaped model with a single bend. Only a very small part of this deviation from linearity can be explained by the general flexibility of

RNA double helices, as a fully double-stranded control RNA behaved as a straight rod under these conditions. It is likely that a main contribution stems from the loop regions A and B with their non-conventional base-pairing, which are possibly more flexible than standard RNA double helices. It is also conceivable that the loop regions introduce some degree of inherent bending into the structure.

The construct with a six nucleotide bulge of sequence AC_5 at the hinge between domains A and B, HP2, shows an average bending angle of 100 (±15)° in the V-model. This result implies that the asymmetric bulge alone imposes a deviation of the RNA from the more extended structure of HP1. Similar effects have been found with six nucleotide bulges of A or U bases (Zacharias & Hagerman, 1995a).

However, in construct HP3, in which direct interactions between loops A and B are enabled, the two domains approach each other more closely with a hinge bending angle of 80 (±20)° according to the V-model or 105 (±25)° in a Y-shaped model. This observation suggests that the task of the loop A/B interaction is not so much to impose a bend in the structure, which is already supported by the bulge, but rather to dock the structure into a defined conformation for subsequent catalysis. The structure as defined by TED measurements is in reasonable agreement with molecular modelling studies, which suggest a Y-type model with a bending angle between domains of 80° (Earnshaw *et al*., 1997). It is possible that both V and Y-structures or their intermediates contribute to the distribution of hairpin ribozyme substrate complexes in solution.

It should be noted that the angles measured by TED are necessarily averaged values in several aspects. First, they may arise from either a fixed bend or a junction with increased flexibility, thus reporting on different types of flexure. Second, dichroism decay signals account for all structural species in solution that exhibit significant linear dichroism upon orientation in an electric field. Thus, structurally heterogeneous molecule populations will yield an averaged value for all such species present. For the hairpin ribozyme in particular, such heterogeneous species have been found to be inherent to its global structure as a two-way junction (Esteban *et al*., 1997, 1998). Up to 26% of the complex could be present as an extended conformer, as found for a hairpin ribozyme construct with short terminal helices (Walter *et al*. 1999). However, the latter construct exhibits a second distinct band on non-denaturing gels, representative of the extended conformer (K. Hampel & J.M.B., unpublished data), which HP3 did not show (see above). In addition, its catalytic activity will produce 28% cleaved complex at equilibrium with uncleaved complex under some of the employed conditions. By virtue of its long binding arms (each one retained in the 5′ and 3′ cleavage products), the cleaved complex stays intact (data not shown). Both cleaved and uncleaved species remain in similar tertiary conformations (Walter *et al*., 1998, 1999; Hampel *et al*., 1998), but the cleaved form might exhibit more flexibility and, therefore, a higher apparent bending angle. The fact that our constructs appeared homogeneous on non-denaturating gels and that we obtained significant differences between constructs and in comparison to fully double-stranded RNA with only subtle changes in sequence, strongly suggests that the calculated bending angles do represent valuable estimates of the global structure of hairpin ribozymes with extended terminal helices.

Finally, TED experiments at high field strength reveal information on the flexibility of RNA molecules. By introducing low energy levels into the system in the order of the thermal energy, partial stretching of bent structures is possible, implying a low energetic barrier for this process. We estimate that the barrier is not higher than ~1.5 kcal/mol. Thus, the bends imposed by the six nucleotide bulge at the hinge and by the internal loops energetically are rather weak. The presence of formally single-stranded regions also leads to the observed intermolecular interactions at micromolar RNA concentrations, focussing our attention on non-Watson-Crick base-paired regions in RNA as the primary mediators of flexibility and interaction within RNA structure.

Materials and Methods

Preparation and initial characterization of RNA

The 5′ and the different 3′ strands of the two-strand hairpin ribozyme constructs shown in Figure 1(c) and the double-stranded RNA reference were separately transcribed from synthesized, partially double-stranded DNA templates using phage T7 RNA polymerase, basically as described (Milligan & Uhlenbeck, 1989), except that higher NTP concentrations (7.5 mM each) together with inorganic pyrophosphatase were used to increase yields (Cunningham & Ofengand, 1990). After 16 hours at 37°C, reactions were extracted with phenol and the RNA recovered by precipitation in ethanol. Full-length products were isolated by UV shadowing from denaturing 20% polyacrylamide, 8 M urea, gels and were checked for their purity by analytical gel electrophoresis.

To analyze homogeneity and electrophoretic mobility of the two-strand hairpin ribozyme constructs, their 5′ and 3′ strands were annealed as described below. Non-denaturing gel electrophoresis was carried out as described (Chowrira & Burke, 1991) on 10% polyacrylamide gels, either in 100 mM Tris-borate (pH 8.0), 2 mM EDTA or in 40 mM Tris-acetate (pH 7.5), 12 mM $MgCl_2$ (similar conditions as for cleavage), at 10 V/cm for three hours. The double-stranded RNA (0.5 μg/lane from a 2 μM RNA stock solution) was EtBr-stained and photographed.

For characterization of cleavage kinetics, the substrate-bearing 3′ strand of HP3 was dephosphorylated with an excess of calf intestine alkaline phosphatase for one hour at 37°C, phenol/chloroform extracted and recovered by precipitation in ethanol. Subsequently, it could be (5′ -^{32}P)-labelled by phosphorylation with phage T4 polynucleotide kinase and [γ-^{32}P]ATP. To observe cleavage, a

trace (<1 nM) amount of (5′-^{32}P)-labelled 3′ strand was pre-incubated in 50 mM Tris-HCl (pH 7.5), 12 mM $MgCl_2$ for 15 minutes at 25 °C, then added either to 100 nM 5′ strand for *cis*-cleavage or to 100 nM hairpin ribozyme (SV5 EH4 Rz construct; Esteban *et al*., 1997) for cleavage *in trans*. At different time points (up to two hours) samples were taken, stopped by the addition of an equal volume of 90 % formamide, 25 mM EDTA, and heat denatured for two minutes at 95 °C. The radiolabelled cleavage product was separated from uncleaved substrate by denaturing 20 % polyacrylamide gel electrophoresis, quantified, and normalized to the sum of the substrate and product bands using a Bio-Rad Molecular Imager System GS-525.

Buffers and RNA annealing

The buffers were: T-Mg, 50 mM Tris (pH 7.5), 12 mM $MgCl_2$ (same as cleavage buffer); T-Na, 50 mM Tris (pH 7.5), 50 mM NaCl; and T-Na-Mg, 50 mM Tris (pH 7.5), 50 mM NaCl, 12 mM $MgCl_2$. The RNA components of the hairpin constructs were mixed in a 1:1 molar ratio in buffer T-Mg or T-Na. For annealing, the samples were heated in a water bath to 90 °C for 2.5 minutes and then slowly (over one hour) cooled down to room temperature. For measurements in buffer T-Na-Mg, the samples were annealed in buffer T-Na as described above and $MgCl_2$ was added to a final concentration of 12 mM.

Transient electric dichroism measurements

TED was measured in a cell with 5 mm optical pathlength and 5 mm distance between the Pt-electrodes, using a cable discharge instrument with pulses of 200 ns length and automatic data collection (Porschke & Obst, 1991). Transients were recorded at electric field strengths from 40 to 90 kV/cm in 10 kV/cm intervals; at each field strength ten transients were averaged. The averaged transients were corrected for artifacts, mainly cell shock effects, by subtraction of ''buffer transients'', which were measured from buffer only, with all other conditions identical. Exponentials were fitted to the corrected transients using a deconvolution procedure (Porschke & Jung, 1985); the references for deconvolution were birefringence signals measured at the different temperatures from the buffers with 2 M urea added. The exponentials were corrected for the increase of the temperature induced by the field pulses using the standard viscosity/temperature conversion factor. For example, the temperature jump induced by a 70 kV/cm pulse in buffer T-Mg at 20 °C is 1.3 deg. C, which was taken into consideration by a correction of 3.74 % for the standard temperature/viscosity conversion factor.

Bead model simulations

Technical details of the bead models used to simulate the experimental dichroism decay curves were as follows: bead assemblies with overlapping beads of uniform radius were used. The bead diameter was 25 Å, corresponding to an approximate helix radius of 12.5 Å. We used procedures for the hydrodynamic calculations as developed and described (Garcia de la Torre & Bloomfield, 1981; Antosiewicz & Porschke, 1989). The extinction coefficient tensors were calculated by tensorial addition of the components of the helical segments. The structure of the helical segments was assumed to be of the *A*-type, with extinction coefficients for light polarized parallel with and perpendicular to the helix axis of $\varepsilon_{\parallel} = 2281\ M^{-1}\,cm^{-1}$ and $\varepsilon_{\perp} = 8609\ M^{-1}\,cm^{-1}$, respectively. Electric polarizabilities of helices or helical segments were calculated from the equation:

$$\alpha = 3 \times 10^{-37}\, N^2\ [CmV^{-1}] \qquad (1)$$

where N is the number of base-pairs. The increase of α with N^2 has been demonstrated for DNA double helices at different ionic strengths (Porschke, 1997); the factor was adapted to the high ionic strength used in the present investigation. Contributions of individual helical segments were combined by tensorial addition. Permanent dipole moments were calculated with respect to the center of diffusion using effective phosphate charges corresponding to 3 % of the elementary charge. The low value for the residual charge was selected in order to get dipole moments in a range consistent with the experimental data, i.e. dipolar energies not much larger than the *kT*-level. It should be noted that these values describe the charges contributing to the dipole potential at the plane of shear for rotational diffusion (Porschke, 1997). Since detailed atomic models were not developed, the positions of the phosphate charges were approximated as located on the axes of the helical segments. All data are calculated for a temperature of 30 °C and a viscosity of $0.7975 \times 10^{-3}\ kg\ m^{-1}\ s^{-1}$.

Acknowledgments

The technical assistance by Jürgen Wawrzinek is gratefully acknowledged. We used the facilities of the Gesellschaft für wissenschaftliche Datenverarbeitung mbH, Göttingen, for computations. Part of this investigation was supported by the grant Po 335/3-2 of the Deutsche Forschungsgemeinschaft to D.P. and an NIH grant to J.M.B.N.G.W. was supported by a Feodor Lynen fellowship from the Alexander von Humboldt foundation and an Otto Hahn medal stipend from the Max Planck Society. We thank Professors F. Eckstein and E. Westhof for comments on the manuscript.

References

Amiri, K. M. A. & Hagerman, P. J. (1994). Global conformation of a self-cleaving hammerhead RNA. *Biochemistry*, **33**, 13172-13177.

Amiri, K. M. A. & Hagerman, P. J. (1996). The global conformation of an active hammerhead RNA during the process of self-cleavage. *J. Mol. Biol.* **261**, 125-134.

Antosiewicz, J. & Porschke, D. (1988). Turn of promoter DNA by cAMP receptor protein characterized by bead model simulations of rotational diffusion. *J. Biomol. Struct. Dynam.* **5**, 819-837.

Antosiewicz, J. & Porschke, D. (1989). Volume corrections for bead model simulations of rotational friction coefficients of macromolecules. *J. Phys. Chem.* **93**, 5301-5305.

Antosiewicz, J. & Porschke, D. (1995). Electrostatics of hemoglobins from measurements of the electric dichroism and computer simulations. *Biophys. J.* **68**, 655-664.

Antosiewicz, J., Nolte, G. & Porschke, D. (1992). Modes of rotational motion of wormlike chains and the

effect of charges on electrooptical transients. *Macromolecules,* **25**, 6500-6504.
Arnott, S., Hukins, D. W. L., Dover, S. D., Fuller, W. & Hodgson, A. R. (1973). Structures of synthetic polynucleotides in the A-RNA and A′-RNA conformations: X-ray diffraction analyses of the molecular conformations of polyadenylic acid · polyuridylic acid and polyinosinic acid · polycytidylic acid. *J. Mol. Biol.* **81**, 107-122.
Bassi, G. S., Mollegaard, N. E., Murchie, A. I., von Kitzing, E. & Lilley, D. M. (1995). Ionic interactions and the global conformations of the hammerhead ribozyme. *Nature Struct. Biol.* **2**, 45-55.
Burke, J. M., Butcher, S. E. & Sargueil, B. (1996). Structural analysis and modifications of the hairpin ribozyme. *Nucl. Acids Mol. Biol.* **10**, 129-143.
Butcher, S. E. & Burke, J. M. (1994). A photo-cross-linkable tertiary structure motif found in functionally distinct RNA molecules is essential for catalytic function of the hairpin ribozyme. *Biochemistry,* **33**, 992-999.
Butcher, S. E., Allain, F. H. T. & Feigon, J. (1999). Solution structure of the loop B domain from the hairpin ribozyme. *Nature Struct. Biol.* **6**, 212-216.
Cai, Z. & Tinoco, I. (1996). Solution structure of loop A from the hairpin ribozyme from tobacco ringspot virus satellite. *Biochemistry,* **35**, 6026-6036.
Chowrira, B. M. & Burke, J. M. (1991). Binding and cleavage of nucleic acids by the ''hairpin'' ribozyme. *Biochemistry,* **30**, 8518-8522.
Chowrira, B. M., Berzal-Herranz, A. & Burke, J. M. (1991). Novel guanosine requirement for catalysis by the hairpin ribozyme. *Nature,* **354**, 320-322.
Cunningham, P. R. & Ofengand, J. (1990). Use of inorganic pyrophosphatase to improve the yield of *in vitro* transcription reactions catalyzed by T7 RNA polymerase. *Biotechniques,* **9**, 713-714.
Cruse, W. B. T., Saludjian, P., Biala, E., Strazewski, P., Prange, T. & Kennard, O. (1994). Structure of a mispaired RNA double helix at 1.6 Å resolution and implications for the prediction of RNA secondary structure. *Proc. Natl Acad. Sci. USA,* **91**, 4160-4164.
Diekmann, S., Hillen, W., Morgeneyer, B., Wells, R. D. & Porschke, D. (1982). Orientation relaxation of DNA restriction fragments and the internal mobility of the double helix. *Biophys. Chem.* **15**, 263-270.
Dock-Bregeon, A. C., Chevrier, B., Podjarny, A., Johnson, J., de Bear, J. S., Gough, G. R., Gilham, P. T. & Moras, D. (1989). Crystallographic structure of an RNA helix: $[U(UA)_6A]_2$. *J. Mol. Biol.* **209**, 459-474.
Earnshaw, D. J., Masquida, B., Müller, S., Sigurdsson, S. T., Eckstein, F., Westhof, E. & Gait, M. J. (1997). Inter-domain cross-linking and molecular modelling of the hairpin ribozyme. *J. Mol. Biol.* **274**, 197-212.
Esteban, J. A., Banerjee, A. R. & Burke, J. M. (1997). Kinetic mechanism of the hairpin ribozyme. Identification and characterization of two nonexchangeable conformations. *J. Biol. Chem.* **272**, 13629-13639.
Esteban, J. A., Walter, N. G., Kotzorek, G., Heckman, J. E. & Burke, J. M. (1998). Structural basis for heterogeneous kinetics: re-engineering the hairpin ribozyme. *Proc. Natl Acad. Sci. USA,* **95**, 6091-6096.
Feldstein, P. A. & Bruening, G. (1993). Catalytically active geometry in the reversible circularization of ''mini-monomer'' RNAs derived from the complementary strand of tobacco ringspot virus satellite RNA. *Nucl. Acids Res.* **21**, 1991-1998.
Ferre-D'Amare, A. R., Zhou, K. H. & Doudna, J. A. (1998). Crystal structure of a hepatitis delta virus ribozyme. *Nature,* **395**, 567-574.
Fredericq, E. & Houssier, C. (1973). *Electric Dichroism and Electric Birefringence*, Clarendon Press, Oxford.
Friederich, M. W., Gast, F.-U., Vacano, E. & Hagerman, P. J. (1995). Determination of the angle between the anticodon and aminoacyl acceptor stems of yeast phenylalanine tRNA in solution. *Proc. Natl Acad. Sci. USA,* **92**, 4803-4807.
Friederich, M. W., Vacano, E. & Hagerman, P. J. (1998). Global flexibility of tertiary structure in RNA: yeast $tRNA^{Phe}$ as a model system. *Proc. Natl Acad. Sci. USA,* **95**, 3572-3577.
Garcia de la Torre, J. & Bloomfield, V. A. (1981). Hydrodynamic properties of complex, rigid, biological macromolecules: theory and applications. *Quart. Rev. Biophys.* **14**, 81-139.
Gast, F.-U., Amiri, K. M. A. & Hagerman, P. J. (1994). Interhelix geometry of stems I and II of a self-cleaving hammerhead ribozyme. *Biochemistry,* **33**, 1788-1796.
Hagerman, P. J. & Amiri, K. M. A. (1996). ''Hammering away'' at RNA global structure. *Curr. Opin. Struct. Biol.* **6**, 317-321.
Hampel, A. & Tritz, R. (1989). RNA catalytic properties of the minimum (−)sTRSV sequence. *Biochemistry,* **28**, 4929-4933.
Hampel, K. J., Walter, N. G. & Burke, J. M. (1998). The solvent protected core of the hairpin ribozyme-substrate complex. *Biochemistry,* **37**, 14672-14682.
Haseloff, J. & Gerlach, W. L. (1988). Simple RNA enzymes with new and highly specific endoribonuclease activities. *Nature,* **334**, 585-591.
Holbrook, S. R., Cheong, C., Tinoco, I., Jr. & Kim, S. H. (1991). Crystal structure of an RNA double helix incorporating a track of non-Watson-Crick base pairs. *Nature,* **353**, 579-581.
Komatsu, Y., Koizumi, M., Nakamura, H. & Ohtsuka, E. (1994). Loop-size variation to probe a bent structure of a hairpin ribozyme. *J. Am. Chem. Soc.* **116**, 3692-3696.
Leehey, M. A., Squassoni, C. A., Friederich, M. W., Mills, J. B. & Hagerman, P. J. (1995). A noncanonical tertiary conformation of a human mitochondrial transfer RNA. *Biochemistry,* **34**, 16235-16239.
Meyer-Almes, F.-J., Heumann, H. & Porschke, D. (1994). The structure of the RNA polymerase-promoter complex. DNA-bending angle by quantitative electrooptics. *J. Mol. Biol.* **236**, 1-6.
Milligan, J. F. & Uhlenbeck, O. C. (1989). Synthesis of small RNAs using T7 RNA polymerase. *Methods Enzymol.* **180**, 51-62.
Murray, J. B., Terwey, D. P., Maloney, L., Karpeisky, A., Usman, N., Beigelman, L. & Scott, W. G. (1998). The structural basis of hammerhead ribozyme self-cleavage. *Cell,* **92**, 665-673.
Ojwang, J. O., Hampel, A., Looney, D. J., Wong-Staal, F. & Rappaport, J. (1992). Inhibition of human immunodeficiency virus type 1 expression by a hairpin ribozyme. *Proc. Natl Acad. Sci. USA,* **89**, 10802-10806.
Orr, J. W., Hagerman, P. J. & Williamson, J. R. (1998). Protein and Mg^{2+}-induced conformational changes in the S15 binding site of 16 S ribosomal RNA. *J. Mol. Biol.* **275**, 453-464.
Pinard, R., Heckman, J. E. & Burke, J. M. (1999). Alignment of the two domains of the hairpin ribozyme-

substrate complex defined by inter-domain photoaffinity crosslinking. *J. Mol. Biol.* **287**, 239-251.
Pley, H. W., Flaherty, K. M. & McKay, D. B. (1994). Three-dimensional structure of a hammerhead ribozyme. *Nature,* **372**, 68-74.
Porschke, D. (1989). Electric dichroism and bending amplitudes of DNA fragments according to a simple orientation function for weakly bent rods. *Biopolymers,* **28**, 1383-1396.
Porschke, D. (1991). Persistence length and bending dynamics of DNA from electrooptical measurements at high salt concentrations. *Biophys. Chem.* **40**, 169-179.
Porschke, D. (1996). Analysis of chemical and physical relaxation processes of polyelectrolytes by electric field pulse methods: a comparison of critical comments with facts. *Ber. Bunsenges. Phys. Chem.* **100**, 715-720.
Porschke, D. (1997). Macrodipoles–unusual electric properties of biological macromolecules. *Biophys. Chem.* **66**, 241-257.
Porschke, D. & Antosiewicz, J. (1990). Permanent dipole moment of tRNA's and variation of their structure in solution. *Biophys. J.* **58**, 403-411.
Porschke, D. & Jung, M. (1985). The conformation of single stranded oligonucleotides and of oligonucleotide-oligopeptide complexes from their rotational relaxation in the nanosecond time range. *J. Biomol. Struct. Dynam.* **2**, 1173-1184.
Porschke, D. & Obst, A. (1991). An electric field jump apparatus with ns time resolution for electro-optical measurements at physiological salt concentrations. *Rev. Sci. Instrum.* **62**, 818-820.
Porschke, D., Tovar, K. & Antosiewicz, J. (1988). Structure of the Tet repressor and Tet repressor-operator complexes in solution from electrooptical measurements and hydrodynamic simulations. *Biochemistry,* **27**, 4674-4679.
Saenger, W. (1984). *Principles of Nucleic Acid Structure*, Springer, Berlin.
Sarver, N., Cantin, E. M., Chang, P. S., Zaia, J. A., Ladne, P. A., Stephens, D. A. & Rossi, J. J. (1990). Ribozymes as potential anti-HIV-1 therapeutic agents. *Science,* **247**, 1222-1225.
Scott, W. G., Finch, J. T. & Klug, A. (1995). The crystal structure of an all-RNA hammerhead ribozyme: a proposed mechanism for RNA catalytic cleavage. *Cell,* **81**, 991-1002.
Scott, W. G., Murray, J. B., Arnold, J. R. P., Stoddard, B. L. & Klug, A. (1996). Capturing the structure of a catalytic RNA intermediate: the hammerhead ribozyme. *Science,* **274**, 2065-2069.
Shen, Z. & Hagerman, P. J. (1994). Conformation of the central, three-way junction of the 5S ribosomal RNA of *Sulfolobus acidocaldarius*. *J. Mol. Biol.* **241**, 415-430.
Sigurdsson, S. T., Thomson, J. B. & Eckstein, F. (1998). Small ribozymes. In *RNA Structure and Function* (Simons, R. W., ed.), pp. 339-376, Cold Spring Harbor Laboratory Press, Cold Spring Harbor, NY.
Tirado, M. M., Lopez Martinez, C. & Garcia de la Torre, J. (1984). Comparison of theories for the translational and rotational diffusion coefficients of rod-like macromolecules. Application to short DNA fragments. *J. Chem. Phys.* **81**, 2047-2052.
Wahl, M. C., Ban, C., Sekharudu, C., Ramakrishnan, B. & Sundaralingam, M. (1996). Structure of the purin-pyrimidine alternating RNA double helix, r(GUAUAUA)d(C), with a 3′-terminal deoxy residue. *Acta Crystallog. sect. D,* **52**, 655-667.
Walter, N. G. & Burke, J. M. (1998). The hairpin ribozyme: structure, assembly and catalysis. *Curr. Opin. Chem. Biol.* **2**, 24-30.
Walter, N. G., Hampel, K. J., Brown, K. M. & Burke, J. M. (1998). Tertiary structure formation in the hairpin ribozyme monitored by fluorescence resonance energy transfer. *EMBO J.* **17**, 2378-2391.
Walter, N. G., Burke, J. M. & Millar, D. P. (1999). Stability of hairpin ribozyme tertiary structure is governed by the interdomain junction. *Nature Struct. Biol.* **6**, 544-549.
Wegener, W. A., Dowben, R. M. & Koester, V. J. (1979). Time-dependent birefringence, linear dichroism and optical rotation resulting from rigid-body rotational diffusion. *J. Chem. Phys.* **70**, 622-632.
Zacharias, M. & Hagerman, P. J. (1995a). Bulge-induced bends in RNA: quantification by transient electric birefringence. *J. Mol. Biol.* **247**, 486-500.
Zacharias, M. & Hagerman, P. J. (1995b). The bend in RNA created by the *trans*-activation response element bulge of human immunodeficiency virus is straightened by arginine and by Tat-derived peptide. *Proc. Natl Acad. Sci. USA,* **92**, 6052-6056.

Edited by I. Tinoco

(Received 29 September 1998; received in revised form 19 March 1999; accepted 6 April 1999)